An Improved Single-Stage PFC AC/DC Power Supply

Thomas Conway

***Abstract*—This letter describes an enhancement to a previously reported single-stage transformer-leakage-inductance based power-factor-corrected isolated power supply.**

An improved switch timing calculation algorithm is developed to achieve zero current switch on of the active rectifier switches. The algorithm is based on an analytical model of the system relating the gate timing to the input and output voltages and control inputs. Remarkably, a closed form expression for the switch timing can be derived and used to calculate and apply the timings in real-time without the need for high speed measurements or resonant structures.

A prototype 1.25 kW prototype power supply is implemented using the proposed technique and performance measurements presented.

***Index Terms*—AC-DC Power Conversion, Power Factor Correction, Transformer Leakage Inductance, Zero Current Switching.**

I. Introduction

Power factor corrected AC-DC power supplies are increasingly important as many more electronic loads are using the AC grid. There is much research on power factor correction in general [1][2] and active power factor correction using modern power electronics techniques [3] are now commonly deployed. For many applications such as electric vehicle chargers, portable inverter welders and plasma cutters, light weight is an important consideration. The single stage architecture in [4] is based on using a single magnetic core for a transformer whose leakage inductance is used in a step up (boost) configuration.

However, the design in [4] requires hard switching of the switches in the secondary side active rectifier.

In this letter, section II describes operation of the power supply, deriving the new equations for switch timing and power handling capability. A prototype 1.25kW power supply based on the described enhancements is presented in section III.

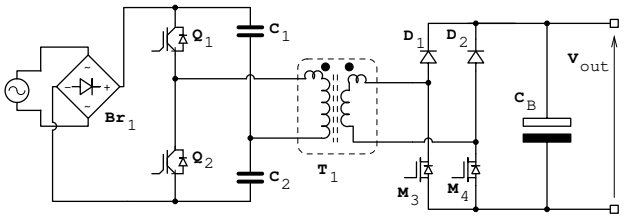

Fig. 1. Circuit diagram of the power supply architecture based on [4].

The circuit diagram of Fig. 1 shows the PFC power supply architecture from [4].

Thomas Conway is a lecturer in the ECE dept. and a researcher with CRIS - the Centre for Robotics & Intelligent Systems (www.cris.ul.ie) at the University of Limerick, Ireland.

Contact: Dr. Thomas Conway ECE Dept, University of Limerick, National Technology Park, Limerick, V94 T9PX, Ireland. Tel +353 61 202628, Email thomas.conway@ul.ie

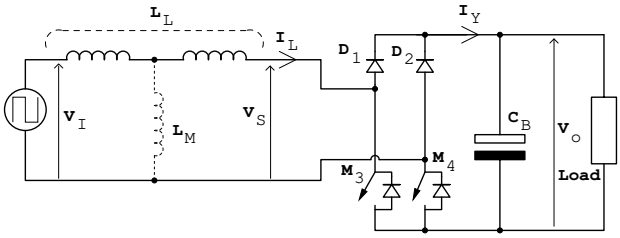

Fig. 2. Simplified circuit model of the power supply.

II. Theory of Operation

A simplified model for the power supply operation is shown in Fig. 2, viewed from the secondary side of the transformer and the magnetizing inductance L_M is assumed sufficiently large to be ignored. The scaled input voltage to the transformer model (V_I) is a square wave at the switching frequency f_s with magnitude $\frac{1}{2}\frac{N_s}{N_p}\left|\sqrt{2}V_{AC}\sin(2\pi f_{AC}kT)\right|$, with V_{AC} the line input rms voltage, f_{AC} the line frequency, k an index integer and $T = 1/f_s$ being the switching period. The transformer turns ratio is $\frac{N_s}{N_p}$ and the half bridge configuration accounts for the additional factor of $\frac{1}{2}$. The active rectifier D1, D2, M3 and M4, allows the transformer secondary to be shorted by turning on both switches M3 and M4 [5]. The inductance L_L is then operated as boost type converter and the input current is controlled to achieve input power factor correction.

A discontinuous conduction mode (DCM) and continuous conduction mode (CCM) can be identified dependent on whether the inductor current I_L returns to zero in each half period $T/2$ as detailed in [4]. The discontinuous conduction mode inherently provides for zero current switch on of the shorting switches M3 and M4 and no recovery losses in the diodes D1 and D2, but the continuous conduction mode requires switch on with non zero current values and hard turn off of the diodes with the associated recovery loss.

A. Gate timing for zero current switch on of M3/M4

In this letter, zero current switch on of M3 and M4 is achieved in the CCM mode by delaying the switch on time to a period T_0 after the transformer primary voltage changes polarity. Fig. 3 shows the detailed CCM mode waveforms. At $t = 0$, the scaled transformer primary voltage changes polarity from $-V_I$ to $+V_I$ with the transformer secondary having a current of $-I_E$ and M3 and D2 are conducting. The transformer secondary current flowing through the inductance L_L, decays to 0 over the period T_0. With the output voltage

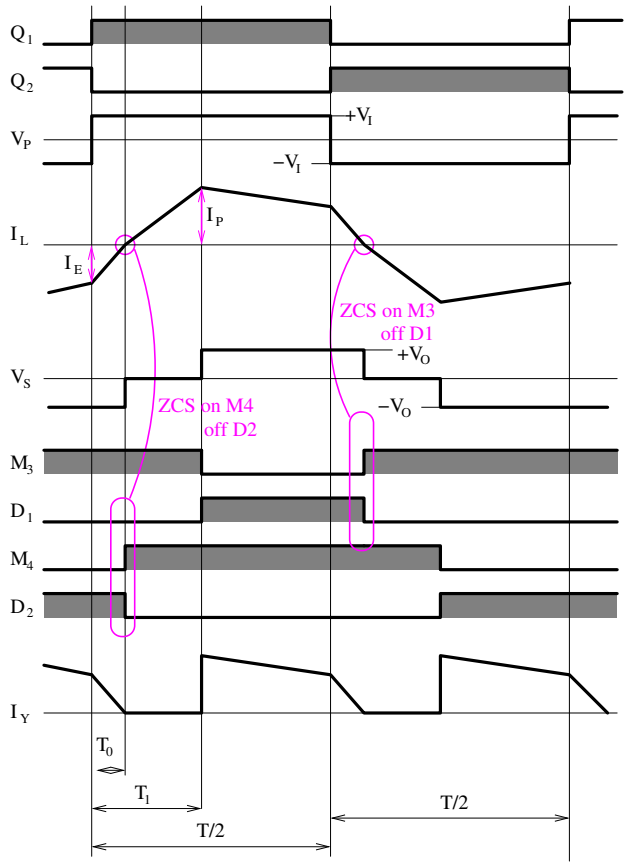

Fig. 3. Waveforms for continuous conduction mode with zero current switching on M3 and M4.

V_O, then the inductor current from $t = 0$ to $t = T_0$ is governed by the equation:

$$0 = -I_E + \frac{(V_I - (-V_O))T_0}{L_L} \tag{1}$$

At the time $t = T_0$, the diode D2 auto-commutes off, and the switch M4 is turned on with zero current, and shorts the transformer secondary. Both M3 and M4 remain on until $t = T_1$, and the current flowing through the leakage inductance L_L rises to a level $+I_P$. Thus, from T_0 to T_1, while shorted:

$$I_P = \frac{V_I(T_1 - T_0)}{L_L} \tag{2}$$

At the time $t = T_1$, M3 is turned off and the inductor current forces diode D1 on. For the rest of the period to $T/2$, current flows through D1 to the output and finishes at level $+I_E$ when $t = T/2$. Thus, after $t = T_1$ to $t = T/2$:

$$I_E = I_P + \frac{(V_I - V_O)(T/2 - T_1)}{L_L} \tag{3}$$

Combining eqn. 1, 2 and 3, yields the set of equations:

$$\begin{aligned} I_E - I_P &= \frac{V_I T}{2L_L} - \frac{V_I T_1}{L_L} + \frac{V_O T_1}{L_L} - \frac{V_O T}{2L_L} \\ I_P + I_E - \frac{T_0 V_O}{L_L} &= \frac{V_I T_1}{L_L} \\ I_P + \frac{T_0 V_I}{L_L} &= \frac{V_I T_1}{L_L} \end{aligned}$$

or writing in matrix form:

$$\begin{bmatrix} 1 & -1 & 0 \\ 1 & 1 & \frac{-V_O}{L_L} \\ 0 & 1 & \frac{V_I}{L_L} \end{bmatrix} \begin{bmatrix} I_E \\ I_P \\ T_0 \end{bmatrix} = \begin{bmatrix} \frac{V_I T}{2L_L} - \frac{V_I T_1}{L_L} + \frac{V_O T_1}{L_L} - \frac{V_O T}{2L_L} \\ \frac{V_I(T_1)}{L_L} \\ \frac{V_I T_1}{L_L} \end{bmatrix} \tag{4}$$

Applying Cramers rule to solve for T_0 yields

$$T_0 = \frac{V_O T_1 + (V_I - V_O)\frac{T}{2}}{V_O + 2V_I} \tag{5}$$

The average input current I_A over a single switching cycle can be calculated as

$$I_A = \frac{-\frac{I_E T_0}{2} + \frac{I_P(T_1 - T_0)}{2} + \frac{(I_P + I_E)(T/2 - T_1)}{2}}{T/2} \tag{6}$$

and to achieve unity input power factor requires this average input current I_A to be proportional to the input voltage V_I or $I_A = G_M V_I$ with G_M being a controlled input transconductance. Substituting $I_A = G_M V_I$ and rearranging gives:

$$\begin{aligned} G_M V_I T L_L &= -V_I T_0 T_1 + \frac{V_O T_0 T}{2} - V_O T_0 T_1 \\ &- V_O T_0^2 + \frac{V_I T_1 T}{2} - V_I T_1 T_0 \end{aligned} \tag{7}$$

To avoid requiring accurate knowledge of the leakage inductance L_L, the modified control variable $K = \frac{G_M L_L}{T}$ is adopted and eqn. 7 becomes

$$K V_I T^2 - V_I T_1 T/2 = V_O T_0 T/2 - V_O T_0 T_1 - V_O T_0^2 - 2V_I T_1 T_0 \tag{8}$$

Using the result of eqn. 5 and expanding the expression into a polynomial in T_1 results in the unwieldy equation of

$$\begin{aligned} &T_1^2\left(-AV_O^2 - 2AV_I V_O - V_O^3\right) + \\ &T_1\left(+AV_O^2\tfrac{T}{2} - 2BV_O^2 - ABV_O - 2ABV_I + A^2 V_I \tfrac{T}{2}\right) \\ &+\left(ABV_O\tfrac{T}{2} - V_O B^2 - A^2 K V_I T^2\right) \quad = 0 \end{aligned} \tag{9}$$

where the expression $(V_O + 2V_I)$ is denoted as A and $(V_I - V_O)T/2$ is denoted as B. Eqn. 9 is a quadratic in T_1 and upon full expansion only the voltage ratio $\frac{V_I}{V_O}$ is present which is henceforth defined as $x = \frac{V_I}{V_O}$. Eqn. 9 can then be written as

$$a\left(\frac{T_1}{T/2}\right)^2 + b\left(\frac{T_1}{T/2}\right) + c = 0 \tag{10}$$

with the coefficients being calculated as:

$$\begin{aligned} a &= -\left(2 + 4x + 4x^2\right) \\ b &= 4 + 4x + 4x^2 \\ c &= x^2 + x - 2 - 4Kx - 16Kx^2 - 16Kx^3 \end{aligned} \tag{11}$$

Thus with measurement of the voltage ratio $x = \frac{V_I}{V_O}$, which varies relatively slowly compared to the switching period T, the coefficients in eqn. 11 can be calculated. Then, the value of T_1 as a ratio of the half switching period $T/2$ can be calculated by solving the quadratic equation in eqn. 10. Furthermore, the value of T_0 as a ratio of the half switching period $T/2$ can then be calculated as

$$\frac{T_0}{T/2} = \left(\frac{\frac{T_1}{T/2} + x - 1}{2x + 1}\right) \tag{12}$$

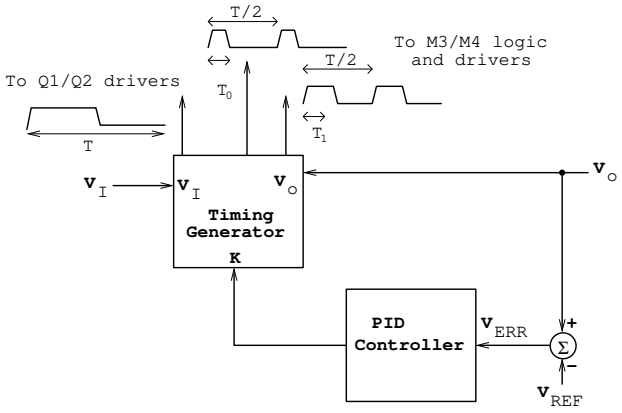

Fig. 4. Output voltage control and timing generation for Q1/Q2 and M3/M4.

Remarkably, eqns. 10, 11 and 12 provide a closed form expression for the switch timings T_0 and T_1, needed to achieve zero current switch on of the shorting switch using only the measured ratio $x = \frac{V_I}{V_O}$ and the control parameter K. While not trivial, these equations can be solved in real-time using a modern DSP, FPGA or custom digital solution. Alternatively, a lookup table indexed on the parameters x and K can be used to calculate T_0 and T_1, in a modern microcontroller. It can also be noted that the calculated T_0 is the minimum value required for zero current switching and this value could be increased to add margin if calculation/measurement precision was an issue. While the turn off of M3/M4 is not changed, their turn off corresponds to turn on of the the diodes D1/D2 which is less of an issue than their turn off recovery losses. The output capacitance of M3/M4 will mitigate the turn off losses of M3/M4 but it was not necessary and was of no benefit to add additional capacitors for this purpose in the prototype.

The output voltage and the timing of the switches are controlled by a low bandwidth feedback control loop as shown in Fig. 4. Transistors Q1/Q2 are switched with a fixed 50% duty cycle at the switching period T. A negative feedback loop uses the output voltage error with a PID controller to control the parameter K. The timing generator uses this value K, and the measured input voltage V_I and output voltage V_O and uses equations eqns. 10, 11 and 12 to calculate the required values for T_0 and T_1. The measurements of V_I, V_O and the solution calculations need to be performed at a rate substantially higher than the AC input frequency, but can be less than the switching frequency f_s. In the prototype, the control loop/timing calculations were operated at a 10kHz rate with a 50kHz switching frequency and 50Hz AC input, though there is considerable scope for increasing the switching frequency and reducing the size/weight of the magnetics particularly with wide band-gap switches (SiC or GaN), and a DSP, FPGA or custom digital solution.

B. Power Handling Capability

The maximum power that can be transferred by the power supply is limited by the requirement that the calculated value of $\frac{T_1}{T/2}$ from eqn. 10 be real i.e. $b^2 \geq 4ac$, and this requires

$$K \leq \left(\frac{1}{4}\right) \frac{1 + 5x + 8x^2 + 4x^3}{1 + 6x + 14x^2 + 16x^3 + 8x^4} \tag{13}$$

giving a maximum power transfer as a function of x as

$$P_{\max}(x) \leq \frac{V_{AC}\frac{N_s}{N_p}V_O}{32\sqrt{2}L_L f_s}\left[4x\frac{1 + 5x + 8x^2 + 4x^3}{1 + 6x + 14x^2 + 16x^3 + 8x^4}\right] \tag{14}$$

With a maximum value of $x = 1$, and the output voltage $V_O = V_I = \sqrt{2}V_{AC}\frac{N_s}{N_p}\frac{1}{2}$, then the maximum output power is

$$P_{\max} = 1.6 \times \frac{V_{AC}\frac{N_s}{N_p}V_O}{32\sqrt{2}L_L f_s} \tag{15}$$

This is a factor of 1.6 higher than the case in [4] with no ZCS in the active rectifier with the same leakage inductance and switching frequency. This increase is due to two factors:

- A higher peak current is achievable as the leakage inductor current decays faster during the period T_0, due to a larger voltage $V_O + V_I$ rather than V_O being across it;
- Some of the remaining energy in the leakage inductor at the end of the period $T/2$ is transferred to the output during the period T_0 rather than all being returned to the input when no ZCS was used.

III. Prototype Design and Measurements

A prototype power supply using the improved ZCS control has been designed targeting a power level of 1.25kW to illustrate the zero current switching as well as operation at a higher power level than the 300W in [4]. An nominal output voltage level of 125V at 10A is chosen with the source being from the 230V $\pm 10\%$ AC grid. The application for such a power supply is based on the use of an array of power supplies being combined to form an electric vehicle battery charger as described in [6]. A series connection of four such power supplies are intended to provide an output voltage range of 50-500V, resulting in the requirement of 125V per supply.

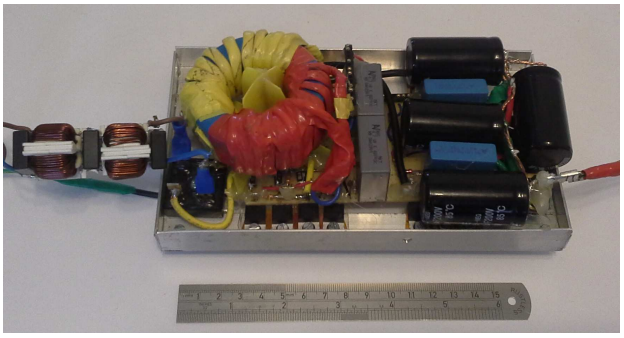

Fig. 5. Prototype 1.25kW power supply.

The turns ratio of the transformer $\frac{N_s}{N_p}$ is determined initially by the requirement for boost operation and thus

$$V_O \geq \frac{1}{2}\sqrt{2}V_{AC}\frac{N_s}{N_p} \tag{16}$$

or with an input AC voltage of 253 Vrms, (230+10%) and minimum output voltage of 125V, the required turns ratio is ≈ 0.714. An actual turns ratio of $\frac{10}{14}$ was used to allow for the voltage drops of the input rectifier, half bridge switches and output diodes.

TABLE I
PROTOTYPE COMPONENT VALUES AND SPECIFICATION.

Component/Parameter	Specified/Measured
EMC filter	3× 100nF Capacitor 2× 5A 7mH Common Mode Choke
Rectifier Br_1	GBPC GPP 50A 600V Bridge Rectifier
IGBTs Q1, Q2	12N60A4D (×4 each) 600V 12A (with diodes)
Capacitors C1, C2	4.7uF 400V Film Capacitor
Transformer	Toroid B64290A0699X087 63mm/38mm dia 25mm height
Turns Ratio	14:10
Primary/Secondary Ind.	900 uH / 432 uH
Sec. Leakage Ind.	8.8 uH
Diodes D1, D2	STTH6002CW 200V 60A (×3)
MOSFETS M3, M4	IRFB4227PBF 200V 65A (×3 each)
Bulk Capacitor	4000uF (4×1000uF) 250V
Control Processor	LPC1114 ARM M0

TABLE II
MEASURED COMPARISON OF PROPOSED SWITCHING AND [4]

	Ref. [4] Switching	Proposed Switching
Max. Power ($V_{AC} = 236V$)	885W	1508W
Measured Efficiency at 885W / 1508W	94.2% / *N/A*	94.5% / 92.5%
Measured Peak Q1/Q2 Current at 885W /1508W	18.5A / *N/A*	16.7A / 30.8A

For a maximum output power to exceed 1.25kW, at the low input voltage of 207 Vrms, (230-10%), the corresponding value of x is 0.836. With a chosen switching frequency of 50kHz, the requirement on the leakage inductance governed by eqn. 14 requires a leakage inductance $L_L \leq 10.8uH$. The transformer is implemented as two separate single layer coils on a toroidal core with the leakage inductance based on [7] and provides a measured leakage inductance of 8.8uH.

A. Measurements and Results

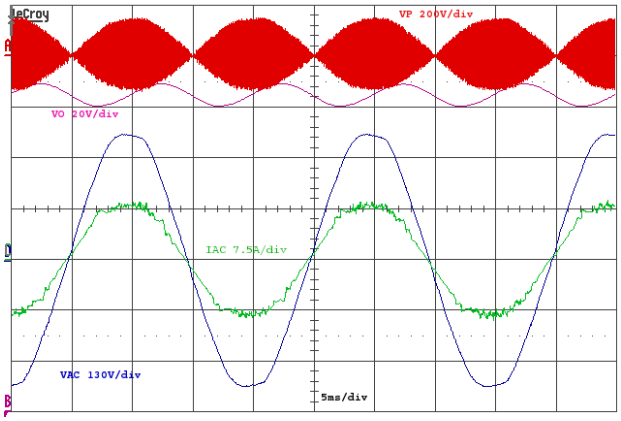

Fig. 6. Measured input current (IAC) and voltage (VAC), output voltage (VO) and transformer primary voltage (VP) at 1.25kW operation.

The power components of the implemented prototype power supply are listed in Table I. Fig. 5 shows a photo of the prototype supply with an external EMI filter. The prototype fits in a volume of 200mm by 100mm by 60mm and weighs 760g. Fig. 6 shows the measured input AC voltage and input current. The current drawn from the grid is sinusoidal and in phase with the input voltage. The measured power factor was 99.8% with 1.25kW output power operation. The output voltage shows an output voltage ripple level of $\pm 5V$ (or $\pm 4\%$) with the output bulk capacitor CB, of 4000uF. The measured transformer primary voltage over a number of 50Hz cycles is also shown and it can be seen that its envelope follows input voltage well even with the half bridge capacitors C1 and C2 being 4.7uF each. Fig. 7 shows the measured transformer primary voltage and current and the secondary voltage and current during the CCM mode of operation at the peak of the AC input voltage and show the zero current switch-on action. The measured performance of the power supply in terms of power factor, efficiency and total harmonic distortion as a function of power level is plotted in Fig. 8 and as function of supply voltage over the range 207V to 264V at 1.25kW and 180V to 264V at 1kW in Fig. 9.

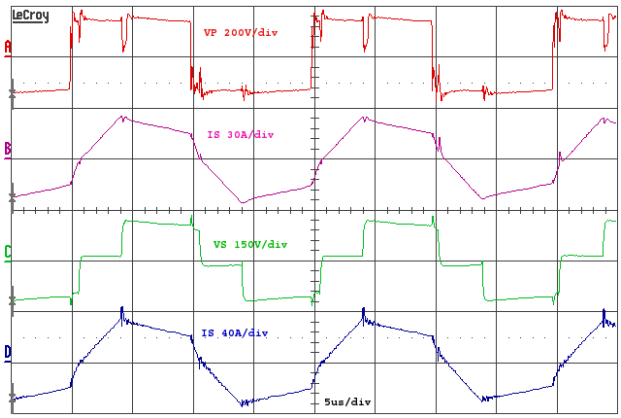

Fig. 7. Measured primary voltage (VP), primary current (IP), secondary voltage (VS) and secondary current (IS) in CCM mode with zero current switch-on of M3 and M4.

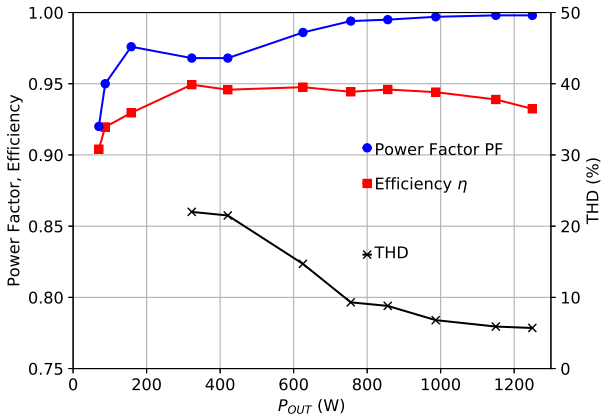

Fig. 8. Measured efficiency, power factor and THD at 230V AC grid voltage.

B. Comparison with Prior Design

The use of the improved timing calculations presented in this letter provides reduces switching losses for turn on of the transistors M3/M4 and turn off/reverse recovery of the diodes

TABLE III
COMPARISON WITH OTHER ISOLATED PFC TOPOLOGIES.

Ref:	Topology	Switching Frequency	Peak Power	Line Voltage	Output Voltage	Cores Weight	Switches (S) Diodes (D)	Peak Efficiency	Power per Core Weight
[8]	Resonant LLC/Boost	90-450kHz	250W	85-265V	48V	92g	8 S , 4 D	94.5%	2.72 W/g
[4]	Single-Stage/Act. Rect.	50kHz	300W	230V	50V	88g	4 S, 6 D	93.7%	3.41 W/g
[9]	Boost/Resonant LLC	100kHz	480W	180-264V	48V	122g	5 S, 4 D	93.58%	3.93 W/g
[10]	Res. Single-Stage	50kHz	1000W	120-240V	360V	190g	2 S, 2 D	97.3%	5.26 W/g
	This work	34-50kHz	1250W	180-264V	125V	240g	4 S, 6 D	95.4%	5.21 W/g

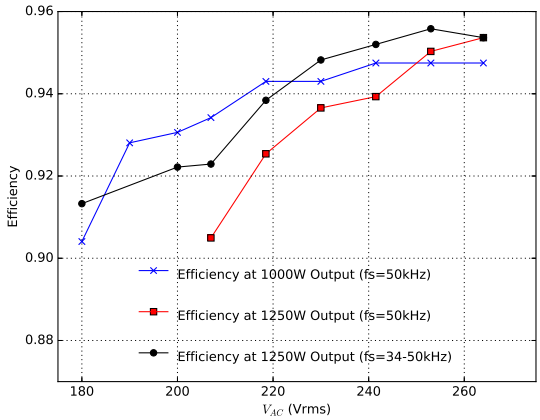

Fig. 9. Measured efficiency against input grid voltage at both 1kW and 1.25kW with fixed f_s = 50kHz and variable frequency operation at 1.25kW with f_s = 34kHz to 50kHz.

D1/D2. As these switching losses represented less than 13% of the total losses, the nominal overall improvement in efficiency is small. However, the improved timing calculations allow a large increase in power handling as shown in section II-B, given a fixed leakage inductance and switching frequency. Table II shows a measured comparison of the the prototype design operation using the original switching scheme of [4] and the switching scheme described in this letter. The maximum power using the original switching scheme in the new prototype is 885W and at this level, the new switching scheme has a slightly improved efficiency of 94.5% versus 94.2% and reduced peak Q1/Q2 current of 16.7A versus 18.5A. The big advantage of the new switching scheme is to allow an increased maximum power level, measured at 1508W with 236Vrms input AC voltage. The peak Q1/Q2 current in this case is measured at 30.8A which is the limiting value imposed by Q1/Q2 in the prototype.

C. Low Voltage Operation

The prototype design is developed for operation from the European voltage range of 230V $\pm 10\%$, but operation at lower voltages is possible at lower power levels and is of general interest. The maximum power operation is determined by eqn. 14, and hence operation at lower voltages should employ a reduced switching frequency f_s. Operation at 1.25kW over the line voltage range 180V to 264V is shown in Fig. 9 using variable frequency operation from 34kHz to 50Khz. Using the prototype hardware and a lower switching frequency of 34.4kHz, the measured maximum power output with a 120Vrms line voltage was 707W with an efficiency of 88.3%. The limiting factor was the Q1/Q2 current limit of 31A and thus higher power operation would require an increased current limit and redesigned transformer.

IV. CONCLUSIONS

An improved timing algorithm is developed to allow zero current turn on of the switches and zero current turn off of the diodes in the in the active rectifier of a single-stage power factor corrected, isolated AC/DC power supply. The developed algorithm allows for real-time calculation of the timing periods by measurement of the input and output voltages and without the need for fast zero current detection or resonant structures.

The prototype 1.25kW supply is compared with a number of designs presented in the literature in table III. The prototype compares well with other reported designs particularly in terms of the peak power and weight of magnetic cores used.

REFERENCES

[1] O. Garcia, J. A. Cobos, R. Prieto, P. Alou and J. Uceda, "Single phase power factor correction: a survey," in IEEE Transactions on Power Electronics, vol. 18, no. 3, pp. 749-755, May 2003.
[2] B. Singh, B. N. Singh, A. Chandra, K. Al-Haddad, A. Pandey and D. P. Kothari, "A review of single-phase improved power quality AC-DC converters," in IEEE Transactions on Industrial Electronics, vol. 50, no. 5, pp. 962-981, Oct. 2003.
[3] M. M. Jovanovic and Y. Jang, "State-of-the-art, single-phase, active power-factor-correction techniques for high-power applications - an overview," in IEEE Transactions on Industrial Electronics, vol. 52, no. 3, pp. 701-708, June 2005.
[4] T. Conway, "An Isolated Power Factor Corrected Power Supply Utilizing the Transformer Leakage Inductance," to appear in IEEE Transactions on Power Electronics. doi: 10.1109/TPEL.2018.2874107
[5] H. Wu, Y. Lu, T. Mu and Y. Xing, "A Family of Soft-Switching DC-DC Converters Based on a Phase-Shift-Controlled Active Boost Rectifier," in IEEE Transactions on Power Electronics, vol. 30, no. 2, pp. 657-667, Feb. 2015.
[6] T. Conway, "BATTERY CHARGING", EP3358698(A1), 2018
[7] F. de León, S. Purushothaman and L. Qaseer, "Leakage Inductance Design of Toroidal Transformers by Sector Winding," in IEEE Transactions on Power Electronics, vol. 29, no. 1, pp. 473-480, Jan. 2014.
[8] L. Gu, W. Liang, M. Praglin, S. Chakraborty and J. Rivas-Davila, "A Wide-Input-Range High-Efficiency Step-Down Power Factor Correction Converter Using a Variable Frequency Multiplier Technique," in IEEE Transactions on Power Electronics, vol. 33, no. 11, pp. 9399-9411, Nov. 2018.
[9] J. I. Baek, J. K. Kim, J. B. Lee, H. S. Youn and G. W. Moon, "A Boost PFC Stage Utilized as Half-Bridge Converter for High-Efficiency DC-DC Stage in Power Supply Unit," in IEEE Transactions on Power Electronics, vol. 32, no. 10, pp. 7449-7457, Oct. 2017.
[10] S. Kim, B. Kwon and M. Kim, "Highly-Efficient Bridgeless Dual-Mode Resonant Single Power-Conversion AC-DC Converter," in IEEE Transactions on Power Electronics. doi: 10.1109/TPEL.2019.2896605